Computer Physics Communications 180 (2009) 1811–1820

Contents lists available at ScienceDirect

Computer Physics Communications

www.elsevier.com/locate/cpc

SPH particle boundary forces for arbitrary boundaries

J.J. Monaghan *, J.B. Kajtar

School of Mathematics Sciences, Monash University, Clayton 3800, Australia

ARTICLE INFO

Article history:
Received 6 November 2008
Received in revised form 20 March 2009
Accepted 10 May 2009
Available online 14 May 2009

Keywords:
SPH
Fluid dynamics
Boundaries

ABSTRACT

This paper is concerned with approximating arbitrarily shaped boundaries in SPH simulations. We model the boundaries by means of boundary particles which exert forces on a fluid. We show that, when these forces are chosen correctly, and the boundary particle spacing is a factor of 2 (or more) less than the fluid particle spacing, the total boundary force on a fluid SPH particle is perpendicular to boundaries with negligible error. Furthermore, the variation in the force as a fluid particle moves, while keeping a fixed distance from the boundary, is also negligible. The method works equally well for convex or concave boundaries. The new boundary forces simplify SPH algorithms and are superior to other methods for simulating complicated boundaries. We apply the new method to (a) the rise of a cylinder contained in a curved basin, (b) the spin down of a fluid in a cylinder, and (c) the oscillation of a cylinder inside a larger fixed cylinder. The results of the simulations are in good agreement with those obtained using other methods, but with the advantage that they are very simple to implement.

1. Introduction

Smoothed particle hydrodynamics (SPH) is a flexible robust method for simulating problems involving fluids interacting with rigid or elastic bodies (for a general reference see [12]). Despite its widespread application the appropriate modelling of boundaries, fixed or moving, is still not clear. For example, in most SPH simulations the boundaries of rigid bodies have been modelled by using either (a) ghost particles, (b) fluid particles, (c) normalizing conditions or (d) boundary particle forces. All of these have advantages and disadvantages.

Ghost particles [3] are similar to the ghost cells used in finite difference calculations. These ghost cells are outside the fluid but alongside the boundary. They have the same density, pressure and temperature as the real cells on the fluid side of the boundary (assumed linear or flat), but with the perpendicular component of the velocity having the opposite sign, and the tangential component having the same sign (free slip) or opposite (no slip). If there is a external force on the fluid the pressure in the ghost cell may need to be adjusted. The properties of SPH ghost particles are obtained from the real SPH particles in the same way as they are obtained for ghost cells. The disadvantage of these ghost cells or ghost particles is that when the boundary changes direction sharply it is not clear how the ghost cells should be placed. For example, if the boundary has a saw tooth configuration, and the teeth are sharp with acute angles, the image cells can be in the fluid on the opposite side of the tooth. A further problem arises if a container with a zig-zag boundary contains two fluids. The position of the ghost particles or cells then depends on the position of the interface between the fluids and it is not clear how they should be placed.

If the boundaries are replaced by fluid particles, as in (b), at least two problems arise. The first is that when fluid moving away from the boundary, as in flow over a weir, the apparent density and pressure decreases, and the particles feel an attraction to the liquid particles on the boundary contrary to the effect of a real boundary. The second is that, when there is more than one fluid, the boundary particles must either be chosen to be one of the fluids throughout the calculation, or they are changed depending on which fluid interacts with them. Not only is this complicated but it is untested.

An alternative method is the option (c) due to Feldman and Bonet [4] who obtain the SPH density by summing over the particles and correcting the summation by a normalizing function near a surface. This normalizing function corrects for the absence of particles beyond the boundary. If this normalizing condition is included in the Lagrangian of the system extra forces appear in the equations of motion. These forces act normal to the surfaces, and increase from zero as the surface is approached from the direction of the fluid. In the case of fixed surfaces this method works well, but in more complicated situations it can be cumbersome. For example, consider a flow containing several bodies which can interact, and imagine two of the bodies in rolling and sliding contact near a corner of one of the bodies. The normalizing function is different for every configuration of the bodies and its evaluation is costly, especially in three dimensions.

The use of normal forces as in option (d) can be traced back to the work of Sirovich [17,18] who formulated the boundary condi-

* Corresponding author.
E-mail address: joe.monaghan@sci.monash.edu.au (J.J. Monaghan).

0010-4655/$ – see front matter
doi:10.1016/j.cpc.2009.05.008

tions between a rigid surface and a fluid as a force in the acceleration equation of the fluid in the form

$$\sigma_{ij} n_j \delta(S), \tag{1.1}$$

where σ_{ij} is the stress tensor in the fluid, n_j is the jth component of the normal to the surface directed towards the fluid, and $\delta(S)$ is a delta function defined with respect to a surface S in the following way.

For any quantity $A(\mathbf{r})$

$$\int A\delta(S)\, d\mathbf{r} = \int A\, d\mathbf{S}, \tag{1.2}$$

where the first integral is over the volume and the second integral is over the surface. In this way a volume integral involving a delta function becomes equivalent to a surface integral, and the force per unit volume in (1.1) becomes a force per unit area. This force provides the pressure which prevents penetration of the rigid body, and the viscous traction term. It mimics the fundamental molecular basis of the boundary conditions namely that the atoms of the fluid do not penetrate the atoms of the solid because of the atomic forces between the liquid and the solid atoms.

A closely related method of using boundary forces is due to Peskin [15] who simulated elastic membranes such as the heart interacting with a fluid. Peskin's equations (2.3) to (2.6) are essentially those of Sirovich, though the Peskin deals with an elastic material and Sirovich assumes the body is rigid. Further details about Peskin's formulation can be found in Peskin [16]. Boundary forces were used by Monaghan [8] in the first application of SPH to the flow of incompressible bodies. The particular form of the forces was chosen to be similar to the Lennard-Jones forces of molecular dynamics. These forces are unsatisfactory because a fluid particle moving past the surface, and keeping a constant distance from it, can feel a non-uniform normal force and a non-zero tangential force. Because of this defect later calculations used boundary particle forces which were normal to the boundary together with a tangential factor which resulted in the force acting on a fluid particle depending only on its perpendicular distance from the boundary [11]. Results from this method were satisfactory though not as good as ghost particles for straight line boundaries in two dimensional flow. Furthermore, the use of normals is not satisfactory for boundaries which are concave relative to the fluid. The fundamental reason is that the normals can cross so that the direction is ambiguous.

In this paper we achieve suitable boundary forces by using radial forces. These forces are sufficiently smooth to ensure that, when the force on a fluid particle is obtained by summing over the boundary particle forces, the final result is independent of the discrete nature of the boundary to a high degree of accuracy. We first establish this result for straight line boundaries in two dimensional configurations by using the Poisson summation formula to relate the force on a fluid particle due to the boundary forces to an integral. This integral is an accurate approximation to the summation provided the spacing of the boundary particles is a factor 2 less than the spacing of the fluid particles. Under these circumstances we then show that the force on the fluid particle is dependent only on the perpendicular distance of the fluid particle from the surface. We then confirm this result by direct summation of the boundary particle forces for boundaries which are straight lines, or circles, with the fluid particle inside or outside the circle (equivalent to a concave or convex boundary). For the case of three dimensional flow we confirm the accuracy of the radial boundary forces by applying them to planar and cylindrical surfaces. We then derive analytical expressions for the pressure and viscous forces exerted on a surface. Finally we apply the radial boundary forces in two dimensional flow problems involving fixed and moving boundaries. The first of these is fluid in equilibrium in a rectangular tank. The second is the buoyant rise of a cylinder in a basin of water. The third is the spin down of a fluid in a cylinder, and the fourth is a cylinder oscillating in a fluid inside another cylinder. Our results are in very good agreement with either exact solutions or with those of other authors using finite difference methods.

2. Boundary force summation and integrals

We begin by considering a two dimensional flow with a boundary which is an infinite straight line, and we calculate the force/mass on a fluid particle a, at a distance y_a perpendicular to the line. We assume the line is the x axis of a Cartesian coordinate system. The x and y components of the force/mass are given by

$$f_x = \sum_{j=-\infty}^{\infty} \frac{(x_a - x_j)}{r_{aj}} \Phi(r_{aj}, h), \tag{2.1}$$

and

$$f_y = \sum_{j=-\infty}^{\infty} \frac{y_a}{r_{aj}} \Phi(r_{aj}, h), \tag{2.2}$$

where r_{aj} is the distance between SPH fluid particle a and boundary particle j. h is a length scale $\sim dp$, where dp is a typical particle spacing. The y coordinate of the boundary particles is zero. The force is along the radial direction and its magnitude is given by the function Φ. We assume the boundary particles are equi-spaced with spacing Δ so that $x_j = j\Delta$.

In order to use the Poisson summation formula consider a generic summation of the form

$$S = \sum_{j=-\infty}^{\infty} \Gamma(j\Delta). \tag{2.3}$$

The Poisson summation formula allows us to estimate this summation from

$$\Delta \sum_{j=-\infty}^{\infty} \Gamma(j\Delta) = \int_{-\infty}^{\infty} \Gamma(q)\, dq + 2\sum_{n=1}^{\infty} \int_{-\infty}^{\infty} \Gamma(q) \cos(2\pi nq/\Delta)\, dq. \tag{2.4}$$

Accordingly, if the Fourier transform of the function $\Gamma(q)$ decreases sufficiently rapidly, the summation on the right-hand side of (2.4) can be neglected and S can be approximated by the integral. For example, if

$$\Gamma(q) = \frac{1}{h\sqrt{\pi}} \exp\left(-q^2/h^2\right), \tag{2.5}$$

then the first integral on the right-hand side of (2.4) has the value 1. The remaining integrals in the summation can be evaluated using

$$\frac{1}{h\sqrt{\pi}} \int_{-\infty}^{\infty} e^{-q^2/h^2} \cos(2\pi nq/\Delta)\, dq = e^{-(n\pi h/\Delta)^2}. \tag{2.6}$$

This shows that provided $\Delta < h$ the successive terms in the summation on the right-hand side of (2.4) decrease very rapidly and are negligible compared with the first integral. The same behaviour occurs for other smooth functions used as interpolation kernels in SPH simulations.

Using these results we can replace the force on a particle due to the boundary force particles by an integration when the boundary

is a straight line. Thus the x component of the force/mass (2.1) becomes

$$f_x = \sum_{j=-\infty}^{\infty} \frac{(x_a - j\Delta)}{r_{aj}} \Phi(r_{aj}) = \frac{1}{\Delta} \int_{-\infty}^{\infty} \frac{(x_a - q)\Phi(r')}{r'}\, dq, \tag{2.7}$$

where

$$r' = \sqrt{(x_a - q)^2 + y_a^2}. \tag{2.8}$$

By setting $q' = x_a - q$, it is clear that this integral vanishes because it is an odd function of q'. To this approximation the x, or tangential component of the force can be neglected because the other terms in the Poisson summation formula are negligible. The y component of the force/mass becomes

$$f_y = \frac{y_a}{\Delta} \int_{-\infty}^{\infty} \frac{\Phi(r')}{r'}\, dq', \tag{2.9}$$

where

$$r' = \sqrt{q'^2 + y_a^2}. \tag{2.10}$$

The integral is, in general, non-zero and has a value independent of x_a. Its dependence on y_a depends on the form of the function Φ. For example, if Φ is a cubic spline which vanishes if its argument is greater than a length scale $2h$, the integrand will be zero everywhere if $y_a > 2h$ and the force will vanish.

3. Tests of the perpendicular and tangential forces

When the boundaries are more complicated than straight lines the simplest way to test the ability of the radial boundary forces to mimic a perpendicular force is to use direct summation. In this section we evaluate the normal and tangential forces by direct summation for particles on straight lines, circles, planes and cylinders. We take $\Phi(\mathbf{r})$ to be given by

$$\Phi(\mathbf{r}) = \frac{W(\mathbf{r})}{|r - d|}, \tag{3.1}$$

where W has the form of a SPH smoothing kernel. The bulk of the tests were completed with d zero, but in the applications we noticed that, under extreme circumstances, a fluid particle could penetrate the boundary at the mid-way point between two boundary particles. At this point the normal components of the boundary forces are zero. Penetration can be prevented by taking d equal to Δ, the boundary particle spacing. With this choice the fluid particle feels an arbitrarily large boundary force as its radial separation from a boundary particle approaches d. We show that the effect of the shift d on the smoothness of the function, and therefore the accuracy with which it mimics a normal force, is negligible.

The kernels we use are the cubic spline, the quintic spline, and the Wendland C2 and C4 kernels [19]. The cubic spline has the form

$$W(q) = \begin{cases} \sigma_3\big[(2-q)^3 - 4(1-q)^3\big], & \text{for } 0 \leqslant q \leqslant 1, \\ \sigma_3(2-q)^3, & \text{for } 1 \leqslant q \leqslant 2, \\ 0, & \text{for } q > 2, \end{cases} \tag{3.2}$$

where $q = |\mathbf{r}|/h$. When the cubic spline is used for interpolation in fluid dynamics σ_3 is chosen so that the integral of $W(q)$ over the relevant space is 1. This is required to ensure that the SPH summations interpolate accurately. However, as noted above, there are different constraints on the boundary forces. For example they should be normal to the boundaries, and prevent particles penetrating the boundary. In this section, where the ratios of the tangential and normal forces, and the ratios of the variation of the normal force to the normal force are calculated, the multiplying constants such as σ_3 are irrelevant. In Section 4 we discuss the values of σ_3 required to keep the fluid SPH particles a distance $\sim dp$ from the boundaries. These remarks apply to the other kernels we consider below.

The quintic spline has the form

$$W(q) = \begin{cases} \sigma_5\big[(3-q)^5 - 6(1-q)^5 + 15(1-q)^5\big], & \text{for } 0 \leqslant q \leqslant 1, \\ \sigma_5\big[(3-q)^5 - 6(2-q)^5\big], & \text{for } 1 \leqslant q \leqslant 2, \\ \sigma_5(3-q)^5, & \text{for } 2 < q > 3, \\ 0, & \text{for } q > 3. \end{cases} \tag{3.3}$$

The Wendland kernels are simpler. They were originally defined so that they vanished for argument > 1. Here they are rescaled to vanish for argument > 2. Wendland uses a notation which depends on the continuity of the function at the origin. In this paper we will refer to the kernels in terms of the dimension of the space and the power of its zero. Thus the one dimensional Wendland kernel C2 which has the form

$$W(q) = \begin{cases} w_3\big(1 + \frac{3}{2}q\big)(2-q)^3, & \text{for } 0 \leqslant q \leqslant 2, \\ 0, & \text{for } q > 2 \end{cases} \tag{3.4}$$

will be referred to as the Wendland 1D cubic. Correspondingly, the Wendland C4 kernel

$$W(q) = \begin{cases} w_5\big(1 + \frac{5}{2}q + 2q^2\big)(2-q)^5, & \text{for } 0 \leqslant q \leqslant 2, \\ 0, & \text{for } q > 2 \end{cases} \tag{3.5}$$

will be referred to as the Wendland 1D quintic. The constants w_3 and w_5 can be chosen in the same way as σ_j. Note that the C2 function is similar in its analytic properties to the cubic spline and the C4 function similar to the quintic spline. Kernels for spaces up to five dimensions are given by Wendland [19].

We scale the spacing of the boundary particles in terms of the perpendicular distance of a fluid SPH particle from the surface. This distance can be thought of as a typical spacing of the fluid SPH particles dp. The maximum variation in the normal force, and the magnitude of the tangential force, both relative to magnitude of the perpendicular component of the force, were calculated for changes in the fluid particle position tangential to the surface. Ideally the variation in the normal force should be zero and the tangential force should be zero. We find these variations are typically $< 10^{-5}$.

3.1. 1D boundaries

In Table 1 we show the maximum absolute value of the ratio of the tangential force to the perpendicular force for the kernels. The distances are scaled in terms of a typical fluid particle spacing. With this scaling the boundary particles were placed along the boundary with spacing equal to $1/\beta$. The boundary force on a test particle with $y = 0$ was sampled at a series (typically 20) of equi-spaced x coordinates between one boundary particle and the next.

The maximum tangential force becomes smaller as β increases (expected because the summation is closer to the integration). For the cubic spline the tangential force is $<10^{-5}$ the perpendicular force provided β is 4 or greater. On the other hand, for the smoother quintic spline, the tangential force is $\leqslant 10^{-7}$ the perpendicular force provided $\beta \geqslant 3$. The error decreases rapidly with β in the case of the quintic spline and the Wendland 1D quintic kernel as expected because their Fourier transforms decrease rapidly. For most computing purposes it is reasonable to work with $\beta = 3$ for the cubic kernels and $\beta = 2$ for the quintic kernels.

In Table 2 we show the maximum variation in the perpendicular force relative to its average value. The results are similar to

Table 1
The maximum absolute value of the ratio of the tangential force to the perpendicular force when the boundary particles are on a straight line. The notation is: β: ratio of the fluid particle spacing to the boundary particle spacing, CS: cubic spline, QS: quintic spline, W3: Wendland 1D cubic, W5: Wendland 1D quintic. The forces are calculated at one fluid particle spacing perpendicular to the line and a series of positions parallel to the line. The shift d is zero.

	Straight line boundary			
	max(tang/perp)			
β	CS	QS	W3	W5
2	9×10^{-5}	4×10^{-5}	5×10^{-5}	5×10^{-5}
3	2×10^{-5}	1×10^{-7}	1×10^{-5}	5×10^{-7}
4	6×10^{-6}	1×10^{-8}	7×10^{-8}	4×10^{-8}

Table 2
The maximum of the ratio of the variation in the perpendicular force to the average perpendicular force when the boundary particles are on a straight line. The notation is the same as in Table 1.

	Straight line boundary			
	max(dperp/perp)			
β	CS	QS	W3	W5
2	1×10^{-4}	2×10^{-5}	4×10^{-5}	5×10^{-5}
3	2×10^{-5}	1×10^{-7}	3×10^{-6}	6×10^{-9}
4	2×10^{-6}	5×10^{-10}	2×10^{-6}	4×10^{-8}

Table 3
The maximum of the ratio of the variation in the perpendicular force to the average perpendicular force when the boundary particles are on a straight line and the shift $d=1/\beta$. The notation is the same as in Table 1.

	Straight line boundary	
	max(tang/perp)	
β	CS	QS
2	3×10^{-4}	1×10^{-5}
3	2×10^{-5}	2×10^{-7}
4	2×10^{-6}	9×10^{-10}

those in Table 1 with very high accuracy being achieved for the smoother kernels with $\beta=3$. Once the ratio becomes very small erratic changes can occur. For example, the values for the W5 kernel for $\beta=3$ are smaller than those for $\beta=4$. These effects may be due to the very small higher order terms in the Poisson summation. In any case the variation in the perpendicular force is very small once $\beta=3$.

In Table 3 we show the maximum absolute value of the ratio of the tangential force to the perpendicular force for the cubic and quintic spline kernels when $d=1/\beta$. The ratios here are larger than those given in Table 1, but they are still very small when $\beta\geqslant3$. These results also indicate that we can expect to get a normal force when $1/(r-d)$ in (3.1) is replaced by another function which is analytic at the position of the test fluid particle.

We now consider concave and convex curved surfaces. Since the local curvature of a line can, in most cases be replaced by that of a circle, we consider circles. The boundary particles were placed at equal intervals around the circumference of the circle separated by a distance as close as possible to $1/\beta$. The test positions, where the force was calculated, were on a circle with radius $R\pm1$ where R is the radius of the boundary particle circle. In the former case the surface is concave relative to the fluid, and in the second case it is convex. We take $d=0$. Tests show that when $d=1/\beta$ the results are similar to those for $d=0$.

Tables 4 and 5 give the same information for a circular boundary of radius 10 as Tables 1 and 2 give for the straight line boundary. As in those cases the tangential force is very small for $\beta\geqslant3$, whether or not the surface is treated as concave or convex. Table 6 gives the same information as for Table 4 but for a circular boundary of radius 2.5. Despite the radius being relatively small compared to the distance of the test points from the boundary the tangential force is still remarkably small. The variation in the perpendicular force, which is not shown here, is similar to that in Table 5.

Table 4
The maximum of the ratio of the tangential force to the average perpendicular force when the boundary particles are on a circle of radius 10. The notation is the same as in Table 1. For each β there are two lines of data. The upper is when the fluid particle is placed a radial distance 1 outside the circle and the lower is when it is placed inside the circle a distance 1. The shift d is zero.

	Circle boundary-radius 10			
	max(tang/perp)			
β	CS	QS	W3	W5
2	1×10^{-4}	4×10^{-5}	2×10^{-5}	9×10^{-5}
	1×10^{-4}	4×10^{-5}	4×10^{-5}	2×10^{-5}
3	2×10^{-5}	4×10^{-8}	1×10^{-5}	7×10^{-7}
	1×10^{-5}	3×10^{-8}	7×10^{-6}	3×10^{-7}
4	3×10^{-6}	2×10^{-9}	5×10^{-6}	1×10^{-7}
	3×10^{-6}	9×10^{-9}	3×10^{-6}	7×10^{-8}

Table 5
The maximum of the ratio of the variation in the perpendicular force to the average perpendicular force when the boundary particles are on a circle of radius 10. The notation is the same as in Table 3.

	Circle boundary-radius 10			
	max(dperp/perp)			
β	CS	QS	W3	W5
2	2×10^{-4}	4×10^{-5}	6×10^{-6}	9×10^{-5}
	5×10^{-5}	1×10^{-5}	4×10^{-5}	2×10^{-5}
3	2×10^{-5}	2×10^{-7}	6×10^{-6}	9×10^{-8}
	1×10^{-5}	3×10^{-8}	4×10^{-6}	2×10^{-7}
4	3×10^{-6}	2×10^{-9}	2×10^{-6}	4×10^{-8}
	6×10^{-6}	8×10^{-9}	8×10^{-7}	2×10^{-8}

Table 6
The maximum of the ratio of the variation in the perpendicular force to the average perpendicular force when the boundary particles are on a circle of radius 2.5. The notation is the same as in Table 1.

	Circle boundary-radius 2.5			
	max(tang/perp)			
β	CS	QS	W3	W5
2	2×10^{-4}	2×10^{-4}	2×10^{-4}	3×10^{-4}
	5×10^{-5}	3×10^{-6}	5×10^{-5}	3×10^{-6}
3	1×10^{-5}	7×10^{-7}	2×10^{-5}	6×10^{-7}
	1×10^{-5}	1×10^{-8}	3×10^{-7}	6×10^{-9}
4	1×10^{-5}	3×10^{-8}	6×10^{-6}	2×10^{-7}
	2×10^{-6}	1×10^{-9}	1×10^{-6}	8×10^{-9}

3.2. 2D boundaries

In this section we consider planes and cylinders as characteristic of two dimensional surfaces. In the case of planes, the boundary particles were placed on a grid of squares. The test position was a vertical distance 1 above the surface, and the force was evaluated for a series of test positions on a grid of squares (with side 0.05 that of the boundary particle square) parallel to the surface. The value of the average perpendicular force, the maximum of the ratio of the tangential to the perpendicular force, and the maximum variation in the perpendicular force were calculated as for the 1D cases.

Table 7 is similar to Table 1 except now for a plane and we confine our results to those for the cubic and the quintic splines. The results are very similar to those in Table 1. In particular the tangential force is very small compared to the perpendicular force provided $\beta\geqslant3$. The variation in the perpendicular force, not shown here, is similar.

Table 7
The maximum of the ratio of the variation in the perpendicular force to the average perpendicular force when the boundary particles are on a plane and the shift $d = 0$. The notation is the same as in Table 1.

	Plane: $d = 0$	
	max(tang/perp)	
β	CS	QS
2	4×10^{-5}	1×10^{-5}
3	9×10^{-7}	4×10^{-8}
4	2×10^{-6}	1×10^{-9}

Table 8
The maximum of the ratio of the variation in the perpendicular force to the average perpendicular force when the boundary particles are on a cylinder of radius 10, and the shift $d = 0$. The same notation is used as in Table 4.

	Cylindrical boundary: $d = 0$	
	max(tang/perp)	
β	CS	QS
2	8×10^{-5}	2×10^{-5}
	6×10^{-5}	1×10^{-5}
3	2×10^{-5}	3×10^{-8}
	5×10^{-6}	3×10^{-8}
4	2×10^{-6}	2×10^{-9}
	2×10^{-6}	8×10^{-10}

In the case of a cylindrical surface we place the boundary particles around the cylinder as in the previous section, and along the cylinder with a spacing $1/\beta$. The test positions are on a concentric cylinder either 1 unit greater or less in radius so that the boundary forms a concave or a convex surface.

In Table 8 we show results similar to those in Table 4 but now for a cylinder, and we confine our results to the cubic and quintic splines. As in the case of Table 4, the tangential forces are very small relative to the perpendicular force provided $\beta \geqslant 3$.

The results in this section indicate that the boundary particles with radial forces can mimic normal forces very accurately provided that the spacing of the boundary particles is less than or equal to 1/3 the fluid particle spacing. The extra boundary particles require a relatively small amount of extra computational work which was not noticeable when β was changed from 2 to 4.

4. Bulk forces

In the present section we calculate the total force on a fluid under gravity in two dimensions. The fluid is assumed to be at rest on one side of an infinite straight line boundary with the x axis along the boundary and y perpendicular to it. Gravity acts in the y direction. The fluid SPH particles are arranged in lines parallel to the boundary and spaced by dp with the bottom layer at a distance σ from the boundary. The separation of the boundary particles is denoted by Δ. We calculate the force on the fluid above a length L of the boundary and compare it to the pressure force $g\rho D$ where g is the gravitational acceleration, ρ the density of the fluid, and D is the depth of the fluid.

The force/mass on fluid SPH particle a due to boundary particle j is normally written in the form

$$\mathbf{f}_{aj} = \frac{K}{\beta}\frac{\mathbf{r}_{aj}}{r_{aj}^2} W(r_{aj}/h)\frac{2m_j}{m_a + m_j}, \tag{4.1}$$

where m_a denotes the mass of particle a and m_j that of particle j [11]. In the following we assume all masses are equal to m. The constant β ensures that, if we change the spacing of the boundary particles the force on the fluid is invariant. For example, if the spacing was halved, the number of boundary particles would be twice as great, but this is compensated by β being twice as great. We discuss the constant K later. Because the tangential component of the force is negligible we only consider the perpendicular y component of the force, and we assume y is measured from the boundary. The total force on the fluid particle a due to all boundary particles is then

$$\sum_{j=-\infty}^{\infty} m f_{aj} = \frac{K m y_a}{\beta} \sum_{j=-\infty}^{\infty} \frac{1}{r_{aj}^2} W(r_{aj}/h), \tag{4.2}$$

where $r_{aj}^2 = y_a^2 + (x_a - x_j)^2$.

Each line of fluid particles contains $n_x = L/dp$ fluid particles, and because they have the same value of y they have the same force. The total force on a line is therefore n_x times the force on any particle on the line. We can therefore choose a representative particle with $x_a = 0$, and we write the value of y_ℓ for line ℓ by

$$y_\ell = \sigma + (\ell - 1)\, dp. \tag{4.3}$$

Combining these results we get the total force in the y direction on the fluid above the length L of the boundary is

$$F = \frac{K n_x m}{\beta} \sum_{\ell=1}^{\infty} y_\ell \sum_{j=-\infty}^{\infty} \frac{W(r_{\ell j}/h)}{r_{\ell j}^2} \tag{4.4}$$

where $r_{\ell j}^2 = y_\ell^2 + x_j^2$. We can write (4.4) in the form

$$F = \frac{K n_x m}{\beta \Delta} \sum_{\ell=1}^{\infty} y_\ell \left(\Delta \sum_{j=-\infty}^{\infty} \frac{W(r_{\ell j}/h)}{r_{\ell j}^2} \right), \tag{4.5}$$

and convert the last summation into an integral with little error. The force per unit length L, with $L = n_x dp$, and $m = \rho(dp)^2$ is then

$$\frac{F}{L} = K\rho \sum_{\ell=1}^{\infty} y_\ell \int_{-\infty}^{\infty} \frac{W(r/h)}{r^2}\, dx, \tag{4.6}$$

where $r^2 = y_\ell^2 + x^2$. The typical value of K for SPH calculations is gD where D is the depth of the fluid. Accordingly

$$\frac{F}{L} = gD\rho S, \tag{4.7}$$

where we expect that $S \sim 1$ for $\sigma \sim dp$.

We expect that different forms of $W(q)$ will require different normalizing factors to get the correct value of S when $\sigma = dp$. We find that if $W(q)$ is the 1D Wendland cubic normalized to 1 when $q = 0$, and $\beta = 4$, then $S = 1.16$ when $\sigma = dp$. On the other hand if $W(q)$ is the 1D Wendland quintic normalized to 1.77 when $q = 0$ and $\beta = 4$, then $S = 1.15$ when $\sigma = dp$.

The force per unit length of the boundary should be the same as the force/length we have already calculated. We now consider a section of the boundary of length L and consider lines of fluid particles which are infinitely long, but spaced as before. The force on boundary particle j due to all the fluid particles is

$$m \sum_a f_{ja} = -\frac{Km}{\beta} \sum_{\ell=1}^{\infty} y_\ell \sum_{i=-\infty}^{\infty} \frac{W(r/h)}{r^2}, \tag{4.8}$$

where the sum over i is the sum over the fluid particles on a line and $r^2 = y_\ell^2 + (x_i - x_j)^2$. The force on all boundary particles in this configuration is the same so we can evaluate it for a representative boundary particle with $x_j = 0$, and multiply it by the number of boundary particles $n_b = L/\Delta$. If the summation over i is then multiplied by dp and converted into an integral we find the force per unit length to be

$$gD\rho \sum_{\ell=1}^{\infty} y_\ell \int_{-\infty}^{\infty} \frac{W(r/h)}{r^2}\, dx, \tag{4.9}$$

which is the same as (4.6).

5. Applications

We now consider how accurately the radial boundary forces simulate boundaries in applications to two dimensional viscous flow. The acceleration equation takes the SPH form

$$\frac{d\mathbf{v}_a}{dt} = -\sum_b m_b\left(\frac{P_a}{\rho_a^2}+\frac{P_b}{\rho_b^2}+\Pi_{ab}+R_{ab}\right)\nabla_a W_{ab} + \sum_{k=1}^{N_b}\sum_{j\in S_k}[\mathbf{f}_{aj} - m_j\Pi_{aj}\nabla_a W_{aj}]. \tag{5.1}$$

In this equation the mass, position, velocity, density, and pressure of particle a are m_a, $\mathbf{r}_a$, $\mathbf{v}_a$, ρ_a, and P_a respectively. W_{ab} denotes the smoothing kernel $W(\mathbf{r}_a-\mathbf{r}_b,\bar{h}_{ab})$ and ∇_a denotes the gradient taken with respect to the coordinates of particle a. The choice of h is discussed in detail by Monaghan [7,12]. The summation over the boundary force particles (the double summation in (5.1)) is equivalent to the term (1.1) discussed in the introduction. This force provides the pressure force on the fluid due to the boundary, and the usual no slip viscous boundary conditions. The ability of the boundary force particles to allow the fluid to satisfy this condition is shown by the results of Sections 5.3 and 5.4.

The first summation in (5.1) is over all fluid particles and is the SPH equivalent of the pressure gradient term and the viscous force/mass. The last term in (5.1) is the contribution to the force/mass on fluid particle a due to boundary particles. k denotes a body, and $j\in S_k$ is one of the set of boundary particle label on body k. The viscosity is determined by Π_{ab} for which we choose the form [9,12]

$$\Pi_{ab} = -\frac{\alpha v_{sig}\mathbf{v}_{ab}\cdot\mathbf{r}_{ab}}{\rho_{ab}|\mathbf{r}_{ab}|}. \tag{5.2}$$

In this expression α is a constant, and $\mathbf{v}_{ab}=\mathbf{v}_a-\mathbf{v}_b$ is used. ρ_{ab} denotes the average density $\frac{1}{2}(\rho_a+\rho_b)$. We take the signal velocity $v_{sig}=(c_a+c_b)/2$, where c_a is the speed of sound at particle a. By a calculation similar to that in Monaghan [12] it is found that the kinematic viscosity for the Wendland 2D quartic is given by

$$\nu = \frac{1}{8}\alpha h v_{sig}. \tag{5.3}$$

SPH calculations for shear flow agree very closely with theoretical results using this kinematic viscosity [13].

The pressure is given by

$$P_a = \frac{\rho_0 c_a^2}{7}\left(\left(\frac{\rho_a}{\rho_0}\right)^7-1\right), \tag{5.4}$$

where ρ_0 is the reference density of the fluid. To ensure the flow has a sufficiently low Mach number to approximate a constant density fluid accurately, we determine the speed of sound by $c_s\sim 10V$ where V is the maximum speed of the fluid relative to the bodies. The term R_{ab} is an anti-clumping term [5,10] which acts to prevent SPH particles clustering in pairs during a simulation. The constant $K=0.01c_s^2=V^2$.

In the examples below the time stepping is based on an integrator which is reversible in the absence of viscosity (for details see Kajtar and Monaghan [6]). The time step is the minimum of δt_c and δt_b, where the former is a Courant condition which is the minimum over fluid particles of $h/(2c_s)$, and the latter is the minimum of $|r_{aj}-d|/\sqrt{K}$ over fluid particles interacting with boundary particles.

The form of the SPH continuity equation we use here is

$$\frac{d\rho_a}{dt} = \sum_b m_b\mathbf{v}_{ab}\cdot\nabla_a W_{ab}, \tag{5.5}$$

and the position of any fluid particle a is found by integrating

$$\frac{d\mathbf{r}_a}{dt} = \mathbf{v}_a. \tag{5.6}$$

In the following applications SI units are used.

5.1. Static tank

This first example illustrates how the particles settle down under gravity with the boundary forces when the boundary includes right angled corners. We simulate fluid in a tank of rectangular cross section of width 2.0 and wall height 1.0 with the water depth $D=0.9$. We take $\beta=2$, using the Wendland 1D quintic for the boundary force, and the Wendland 2D quartic for the fluid dynamics. The Wendland 2D quartic kernel, when normalized so that its integral is 1 in two dimensions, is given by (with $q=r/h\leqslant 2$)

$$W(q) = \frac{7}{64\pi h^2}(1+2q)(2-q)^4 \tag{5.7}$$

and vanishes when $q\geqslant 2$. We take $dp=0.02$ and $h=1.5\,dp$ since this gives a slightly more regular particle positions than the choice $h=1.3\,dp$ for the cubic spline. For this problem we take $c_s=10\sqrt{gD}$, where D is the depth of the fluid. The shift d in the force was taken as dp/β, the Reynolds number, defined as $(gD)^{1/2}D/\nu$, was 100. Note that the choice of Reynolds number determines the constant α according to (5.3).

While it is common practice to initialize the density and pressure of the fluid particles by using hydrostatic equilibrium under gravity, we do not do that here because the SPH particles come into equilibrium under both gravity and the boundary forces. We find it simpler to start the SPH particles with their density equal to the reference density and their pressure zero then damp their motion until they reach equilibrium. The damping is produced by a term linear in the velocity in the acceleration equation. In the present case the particle were damped for 2500 steps.

The positions of the particles 1500 steps after damping are shown in Fig. 1. The particles are highly ordered and the separation from the bottom boundary and the side walls is approximately dp in agreement with our estimate of the bulk force. The fluid particle separation from the side walls increases slightly from bottom to top, but this increase is small $\sim dp$. The separation of the top line of particles from the line beneath it is also close to dp except near the walls, but even there the difference in spacing from the bulk fluid is negligible.

In Fig. 2 we show the time variation of the pressure scaled in units of ρgD. In these units the correct pressure is 1.0. We calculate this pressure in a way which mimics the analysis in the

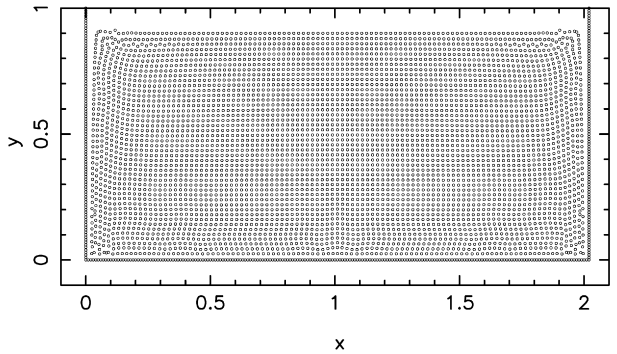

Fig. 1. The positions of SPH particles settled down under gravity in a box where the boundary force is the 1D Wendland quintic. Note the ordered state of the particles, the separation from the bottom boundary (approximately dp) and the fact that, except near the walls, the particles on the surface have a separation of close to the typical separation of particles in the fluid.

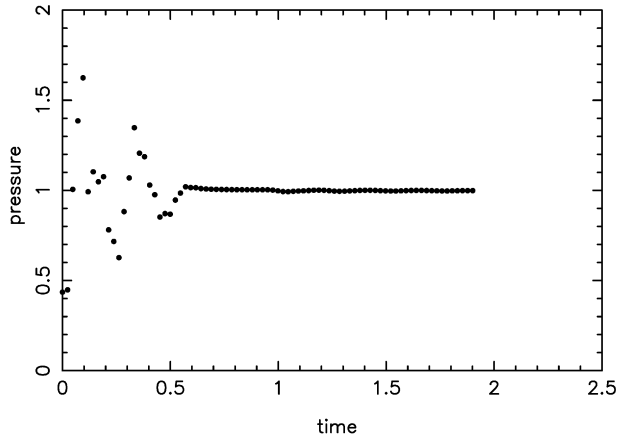

Fig. 2. The time variation of the pressure calculated at the middle point of the bottom of the tank. The pressure is scaled by dividing by $\rho g D$ where D is the depth. The exact value of the scaled pressure is 1.0. The pressure initially fluctuates because the fluid initially has zero pressure. The damping stops at time = 1.0.

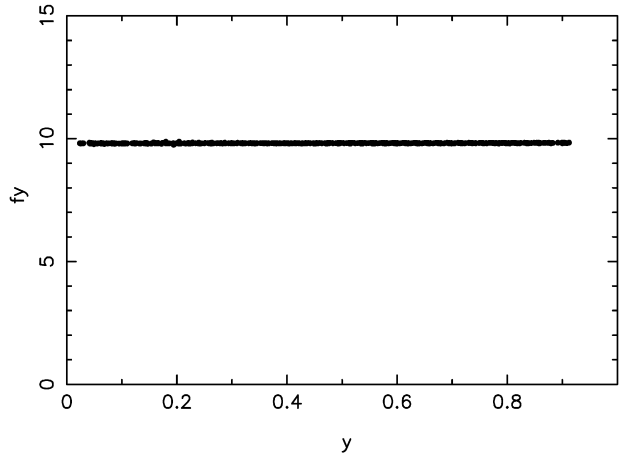

Fig. 3. The variation of the force/mass on each SPH fluid particle in the tank. This force/mass is constant and equal in magnitude to the gravitational acceleration as expected.

previous section. That is we take a length L of the bottom boundary and find the total force F exerted by the fluid on the boundary particles occupying that length. The pressure is then F/L. In Fig. 2 the pressure was calculated for the mid point of the bottom of the tank. Calculations of the time variation of the pressure at x equal to 0.25 and 0.75 the width of the tank gave results that agree with those in Fig. 2 to within 0.1%. These results show that, in agreement with our discussion of the surface force (1.1), the boundary forces correctly determine the pressure exerted by the fluid on the surface, and from the way the forces are constructed (see Section 4.4), this also determines the force exerted on the fluid.

Because the pressure is initially zero the fluid moves down towards the boundary then undergoes damped oscillations. The damping ends at $t = 1.0$. The pressure on the base of the tank from the SPH calculations is in very good agreement with the scaled value of 1.0. In Fig. 3 we show the y component of the force/mass due to the pressure for all fluid SPH particles 2000 steps after damping has ceased. This force should be constant with the same magnitude as the gravitational acceleration 9.806. There are some small deviations from the exact value which show that the system is not quite in equilibrium but these effects are negligible. These results show that the SPH calculation of the pressure gradient is very accurate for this configuration.

5.2. Buoyant rise of a cylinder

The second example we consider is the rise of a cylinder of circular cross section with radius 0.5 in a basin of water with circular cross section of radius 2. The density of the cylinder is 0.8 that of water. The two surfaces within which the liquid moves therefore consists of the concave basin and the convex cylinder. The purpose of this example is to confirm that the boundary particles result in a smooth flow, and to confirm that there is little change in the dynamics as β is increased from 2 to 4. We define the Reynolds number $\mathcal{R}$ of the flow to be $R\sqrt{gR}/\nu$ where R is the radius of the basin. For this calculation $\mathcal{R} = 1000$.

The SPH fluid particles were initially placed on a grid of squares of side $dp = 0.04$ and those inside the outer cylinder, but outside the inner cylinder, were accepted. This procedure results in perturbations around the boundaries, but these are removed by damping as in the previous example. The boundary particles for the cylinder and the basin were placed on the respective boundaries with a spacing Δ as close as possible to dp/β. This was achieved by determining an integer $N = \mathrm{Int}(C/\Delta)$, where C is the circumference of the circle. Δ was then replaced by C/N. The total number of particles when $\beta = 4$ is 4019. The centre of the cylinder was initially a distance 1.0 above the lowest point of the basin and held fixed during the damping. The speed of sound was taken as $10\sqrt{gR}$ where R is the radius of the outer cylinder.

After the damping (carried out in the same manner as in the previous simulation) the equations were integrated for a time = 1.0147. Fig. 4 shows the velocities of the particles at this time. Note that the shape of the cylinder appears altered because the velocity vector of a particle (this includes the boundary particles) starts on the particle. The particle positions and velocities are remarkably regular although they are slightly disordered near the upper surface and below the cylinder where vortices are generated by the flow. The fluid particle separation is nearly constant over most of the fluid though the separation of the two surface layers differs from that in the interior by approximately dp. The surface density is, however, within 10^{-3} of the reference density so that the surface pressure is typically 10^{-4} the pressure at the lowest point of the basin.

In Table 9 we give the values of the y coordinate of the centre of the cylinder at a time 1.0147 after the damping, for three values of β. These results show that there is little change when β is changed from 2 to 4 in agreement with our previous results. However, the change is larger than might be expected from the tests in Sections 2 and 3. Part of this change is due to way the fluid particles were initially placed. They initially have zero pressure and move down under gravity. The particles in the layer adjacent to the bottom of the basin moves very close to the boundary. As a consequence, the time step changes slightly for each choice of β because the boundary particle spacing is different. This alters the configuration of the particles and the sequence of damping. However, the change in position relative to the average position for β equal to 3 and 4 is 1.5×10^{-4}, which is negligible.

5.3. Spin down

The next example is the spin down of a fluid initially rotating rigidly within a container rotating with the same angular velocity then suddenly stopped. The analytical solution can be constructed from the solution given by Batchelor [1]. This example establishes how accurately the boundary forces represent the surface of the cylinder, both in applying a pressure to the fluid, and in representing the viscous interaction. We use the Wendland kernel for two dimensions described in the previous section, and the Wendland 1D cubic function for one dimension (3.4) in the boundary force.

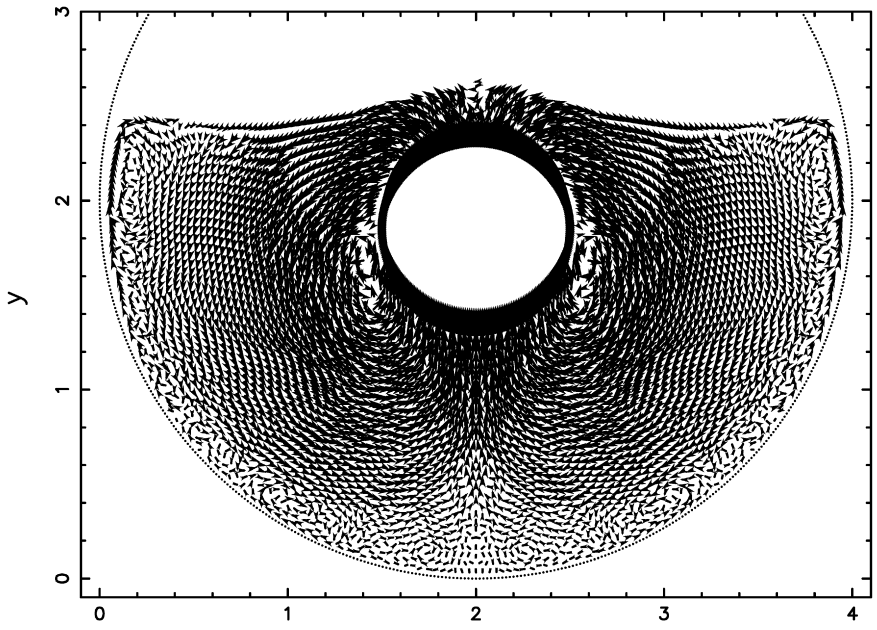

Fig. 4. The velocities of the SPH particles produced by a buoyant cylinder rising in a basin of water of circular cross section.

Table 9
The y coordinate of the centre of the cylinder for various β at a time 1.0147 after the damping ceased.

β	y (cylinder)
2	1.885314
3	1.875001
4	1.874653

The particles were placed on equi-spaced circles with the same spacing in radius around each circumference. For the results in this paper there were 20 circles including the circle of boundary force particles. The radius of the cylinder was $r = 1$ and dp was 0.05. The initial angular velocity was $\Omega = 1$. For these calculations $h = 1.5\,dp$ and $\beta = 3$. The quantity d in the boundary force was equal to Δ. The results to be described were obtained for a Reynolds number $\mathcal{R}$ of 200 defined by

$$\mathcal{R} = \frac{\Omega r^2}{\nu}, \tag{5.8}$$

where the kinematic viscosity is given by (5.3). The speed of sound was 10.

In Fig. 5 we show the azimuthal velocity against radius at a time 0.744 after the cylinder has stopped rotating. There is very good agreement between theory and simulation. Furthermore, since the filled circles in the figure show no sign of being spread, the SPH particles stay on their original circles with very little non-axisymmetric perturbations from the boundary forces. In summary these results show that SPH with radial boundary forces gives very good results for problems involving viscous interaction with a fixed concave surface.

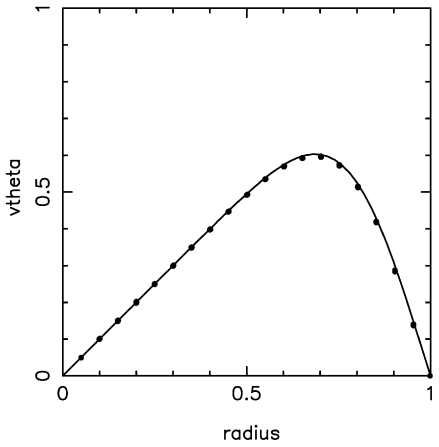

Fig. 5. The variation of azimuthal velocity for the spin down of a fluid at a time 0.744 after the cylindrical container suddenly stopped. The continuous line is the analytical result. The filled circles are the SPH results.

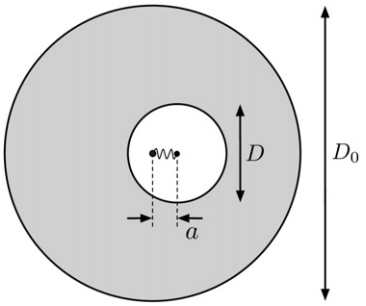

Fig. 6. The setup of a cylinder oscillating within another cylinder. The inner cylinder with diameter D is tethered to the central position of the outer cylinder (of diameter D_0) by a spring. The two black points indicate the centres of the cylinders. Initially the inner cylinder is displaced distance a from the centre. The shaded region represents the viscous fluid.

5.4. A cylinder oscillating within a cylinder

The final example is the motion of a tethered circular cylinder of diameter D and mass M moving through a weakly compressible, viscous fluid inside a cylinder of diameter D_0. This example complements that in the previous section by showing how accurately the boundary force particles represent the pressure and viscous forces acting on the moving body. This example is similar to that considered by Kajtar and Monaghan [6], where the drag and viscous forces on an oscillating cylinder were calculated for an infinite domain and compared against experiment.

The inner cylinder was tethered to the central position of the outer cylinder by an elastic spring with spring constant k_s. The

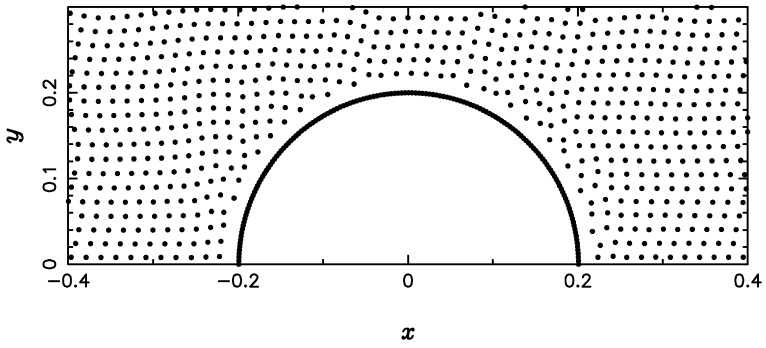

Fig. 7. The particle positions near the inner cylinder at time $t \sim 0.19$. The fluid particles are similarly distributed near the outer cylinder.

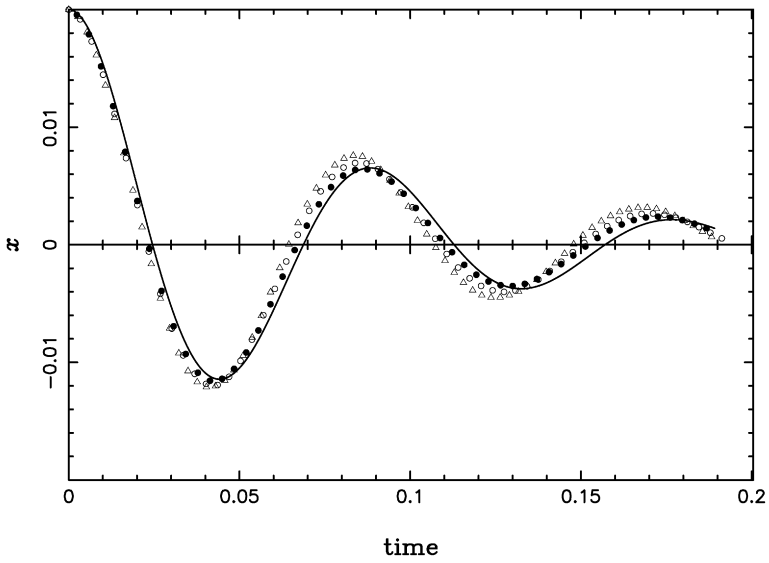

Fig. 8. The position of the centre of mass of the inner cylinder plotted against time. The calculations with three different resolutions are plotted together with the approximate analytical results from Chen et al. shown as a continuous line. The filled circles are the SPH results for $dp = 1/120$, the open circles are for $dp = 1/90$ and the open triangles are for $dp = 1/60$. These results indicate convergence.

setup is shown in Fig. 6. We study the convergence of the calculation and compare our numerical results to the linearized analytical solution given by Chen et al. [2], which is suitable for oscillations with initial displacement a satisfying $a \ll D$.

For these calculations $D_0/D = 5$ and the initial displacement of the inner cylinder was $a = 0.05D$. The errors in Chen's linearized theory are not known, but we take the view that our $a/D = 1/20$ is sufficiently small.

The inner cylinder has diameter $D = 0.4$, density twice that of the fluid, and therefore mass $M = 2\rho_0\pi(\frac{1}{2}D)^2$ where $\rho_0 = 1000$ is the density of the fluid. The spring constant is $k_s = 10000M$ so that the undamped frequency $\omega = 100$. The fluid particles were given an initial over-density $\rho = 1.01\rho_0$, and mass $m = 1.01\rho_0(dp)^2$. We use a Cartesian coordinate system with the origin at the centre of the outer cylinder. The fluid particles were placed on a regular grid of squares within the annular region, and were excluded if their distance from the origin was greater than $D_0 - dp$. Similarly, they were excluded if their distance was less than $D + dp$ from the centre of the inner cylinder.

The particle positions for $dp = 1/60$ with $\beta = 4$ are shown in Fig. 7 for a small region around the inner cylinder at time $\sim$0.19 after the damping. This figure shows that the particles remain regular although there is slight disorder around the cylinder. The positions of the particles near the outer cylinder show a similar disorder. With $\beta = 4$, we ran the calculation for three fluid particle spacings, $dp = 1/60$, $1/90$ and $1/120$. For the highest resolution, the initial displacement of the inner cylinder from the origin was $2.4\,dp$. We set the speed of sound $c_s = 10\omega D$ and the kinematic viscosity $\nu = 0.2$. The Reynolds number $\mathcal{R}$, defined by $\mathcal{R} = \omega_d D^2/\nu$, is $\sim$58. In the definition of $\mathcal{R}$, ω_d is the damped frequency [2].

In Fig. 8 the time variation of the centre of the inner cylinder is shown for the three resolutions and for the analytical theory. The results for the analytical theory require coefficients C_V and C_M which we estimated from Chen's graphs by interpolation with errors $\sim$5%. For the present calculation we find $C_V = 0.97$ and $C_M = 1.83$. Note that the definition of C_V by Chen is ambiguous, but the ambiguity can be resolved by reference to the results of Nomura and Hughes [14]. The graphs in Fig. 8 show that the principal difference between the SPH results and the analytical curve is a shift in phase of approximately 0.005 compared with the period of $\sim$0.09. The difference between the amplitude of the SPH results and the analytical curve is small, and reduces with increased resolution. We regard the agreement between the SPH results and those of Chen as very good considering the initial displacement of the inner cylinder, at the highest resolution, is only $2.4\,dp$.

To determine the effect of changing β for constant resolution we ran the simulation with $dp = 1/90$ and four values of β. The position and time coordinates for the first peak (exactly 1 period after $t = 0$) for different values of β are given in Table 10. These results show that, as expected, the variation due to changes in β is very small.

Table 10
Amplitude and time of the first peak after the oscillation begins for different β.

β	t	x
1	8.54327×10^{-2}	6.94335×10^{-3}
2	8.52332×10^{-2}	6.97803×10^{-3}
3	8.52258×10^{-2}	6.98221×10^{-3}
4	8.52239×10^{-2}	6.98543×10^{-3}

6. Conclusions

We have shown, by analysis and direct summation, that boundary particles interacting with fluid particles through appropriate radial forces result in a total boundary force which is normal to the boundary to high accuracy. The variations in the magnitude of the normal force are also very small, typically $\sim 10^{-5}$. The appropriate radial forces are of the form $W(r)/(r-d)$ where W is any sufficiently smooth function which, in this paper, is one of the cubic and quintic splines, or the Wendland 1D cubic and quintic kernels. The Wendland quintic kernel or the quintic spline reduce the errors by a factor 100 compared to the cubic spline and Wendland cubic.

The boundary particles must have a spacing relative to the fluid particles of $\sim 1/3$ to guarantee that the magnitude of the tangential force relative to the normal force, and the relative variation in the normal force for a fixed distance above the boundary, are both $< 10^{-5}$, but the resulting increased number of particles results in only a small increase in the computing time.

Application to the equilibrium of a static tank shows that the particles are highly ordered with positions that do not differ significantly when the boundary particle spacing is changed. Application to the rise of a buoyant cylinder in a basin tests the boundary forces for convex and concave boundaries. Again the results only change slightly with the spacing of the boundary particles relative to the spacing of the fluid particles. The spin down of a fluid in a cylinder shows that the boundary forces produce the correct viscous boundary stress and the boundary particles produce negligible perturbations to the cylindrical flow. Finally we considered a cylinder oscillating inside another cylinder containing a viscous fluid. Comparison with an approximate analytic solution shows good convergence as the spacing of the fluid and boundary particles is reduced.

These results show that the radial boundary forces discussed in this paper provide a simple and efficient method of handling complex boundaries in SPH simulations.

References

[1] G.K. Batchelor, An Introduction to Fluid Mechanics, Cambridge University Press, London, 1967.
[2] S.S. Chen, M.W. Wambsganss, J.A. Jendrzejczyk, Added mass and damping of a vibrating rod in confined viscous fluids, J. Appl. Mech. (1976) 324–329.
[3] A. Colagrossi, M. Landrini, Numerical simulation of interfacial flows by smoothed particle hydrodynamics, J. Computat. Phys. 191 (2003) 448–475.
[4] J. Feldman, J. Bonet, Dynamic refinement and boundary contact forces in SPH with applications in fluid flow problems, Int. J. Numer. Meth. Eng. 72 (3) (2007) 295–324.
[5] J. Gray, J.J. Monaghan, R. Swift, SPH elastic dynamics, Comput. Method Appl. Mech. Eng. 190 (2001) 6641–6662.
[6] J. Kajtar, J.J. Monaghan, SPH simulations of swimming linked bodies, J. Comput. Phys. 227 (2008) 8568–8587.
[7] J.J. Monaghan, Smoothed particle hydrodynamics, Ann. Rev. Astron. Astro. 30 (1992) 543–573.
[8] J.J. Monaghan, Simulating free surface flows with SPH, J. Comput. Phys. 110 (1994) 399–406.
[9] J.J. Monaghan, SPH and Riemann solvers, J. Comput. Phys. 136 (1997) 298–307.
[10] J.J. Monaghan, SPH without a tensile instability, J. Comput. Phys. 159 (2000) 290–311.
[11] J.J. Monaghan, A.M. Kos, N. Issa, Fluid motion generated by impact, J. Waterways Ports Coast. Ocean. Eng. 129 (6) (2003) 250–259.
[12] J.J. Monaghan, Smoothed particle hydrodynamics, Rep. Progress Phys. 68 (2005) 1703–1759.
[13] J.J. Monaghan, Smoothed particle hydrodynamics simulations of shear flow, Mon. Not. R. Astro. Soc. 365 (2006) 199–213.
[14] T. Nomura, T.J.R. Hughes, An arbitrary Lagrangian–Eulerian finite element method for the interaction of fluid and rigid body, Comput. Method Appl. Mech. Eng. 95 (1992) 115–138.
[15] C.S. Peskin, Numerical analysis of blood flow in the heart, J. Comput. Phys. 25 (1977) 220–252.
[16] C.S. Peskin, The immersed boundary method, Acta Numer. 10 (2002) 479–517.
[17] L. Sirovich, Initial and boundary value problems in dissipative gas dynamics, Phys. Fluids 10 (1967) 24–34.
[18] L. Sirovich, Steady gasdynamic flows, Phys. Fluids 11 (1968) 1424–1439.
[19] H. Wendland, Piecewise polynomial, positive definite and compactly supported radial functions of minimal degree, Adv. Comput. Math. 4 (1995) 389–396.